

Measuring correlated electron dynamics with time-resolved photoemission spectroscopy

Martin Eckstein and Marcus Kollar

*Theoretical Physics III, Center for Electronic Correlations and Magnetism,
Institute for Physics, University of Augsburg, 86135 Augsburg, Germany*

(September 25, 2008)

Time-resolved photoemission experiments can reveal fascinating quantum dynamics of correlated electrons. However, the thermalization of the electronic system is typically so fast that very short probe pulses are necessary to resolve the time evolution of the quantum state, and this leads to poor energy resolution due to the energy-time uncertainty relation. Although the photoemission intensity can be calculated from the nonequilibrium electronic Green functions, the converse procedure is therefore difficult. We analyze a hypothetical time-resolved photoemission experiment on a correlated electronic system, described by the Falicov-Kimball model in dynamical mean-field theory, which relaxes between metallic and insulating phases. We find that the real-time Green function which describes the transient behavior during the buildup of the metallic state cannot be determined directly from the photoemission signal. On the other hand, the characteristic collapse-and-revival oscillations of an excited Mott insulator can be observed as oscillating weight in the center of the Mott gap in the time-dependent photoemission spectrum.

PACS numbers: 71.27.+a, 78.47.-p

I. INTRODUCTION

Pump-probe experiments with femtosecond time resolution can record various nonequilibrium processes in solids directly in the time domain, including those induced by the Coulomb interaction between electrons, or the scattering of electrons on defects and phonons. In these experiments excitation of the sample and characterization of the excited state are accomplished by two distinct laser pulses (pump and probe) which hit the sample with controlled time delay, and either optical or photoemission spectroscopy may be used as probe technique. The pump-probe setup has been used to investigate the dynamics of molecules,¹ semiconductors,² and metals³ for more than two decades. More recently, such time-resolved experiments were also performed on several strongly correlated materials close to a phase transition, where many degrees of freedom contribute to the dynamics on very different time scales.^{4,5,6,7,8,9}

In such nonequilibrium solid-state experiments it is a major challenge to distinguish the electronic dynamics from other degrees of freedom. This is crucial in particular for the Mott metal-insulator transition,¹⁰ which is driven by the Coulomb interaction between electrons moving in a crystal lattice. An entirely new perspective on this phenomenon would open up if one could observe the transition as it happens in real time and, e.g., monitor the formation of well-defined quasiparticles as the system goes from an insulating to a metallic state. In fact, in several Mott and charge-transfer insulators the transition to a metallic state can be induced by a laser pump pulse.^{4,5,7,8} So far these experiments have focused on the relaxation back to the insulating state, which involves coupling to degrees of freedom other than the valence band electrons, and is much slower than the buildup of the metallic state after the pump pulse. In the sim-

plest case the observed relaxation is described by the two-temperature model,¹¹ i.e., as the cooling of a hot electron gas which is coupled to the colder lattice.^{7,12} The true dynamics of the electronic system has so far been observed only in simple metals, by looking at the thermalization of pump-excited electron distributions due to electron-electron scattering.^{3,13} In strongly correlated materials, thermalization is apparently much faster. Sufficient time resolution is now becoming available due to recent advances in femtosecond laser techniques,^{14,15} which have already allowed to investigate some solid-state systems even on the attosecond time scale.¹⁶

In equilibrium, electronic properties of correlated materials can be obtained directly from conventional photoemission spectroscopy with continuous light beams.^{17,18} By contrast, time-resolved measurements are likely to be restricted by the frequency-time uncertainty of the probe pulse: The energy ϵ of occupied states in the solid from which photoelectrons are released is determined from the kinetic energy of the photoelectrons, the work function of the solid, and the photon energy $E_\gamma = \hbar\omega$; when the measurement pulse has finite duration δt , the latter is determined only up to an uncertainty $\delta E_\gamma \gtrsim \hbar/\delta t$. In a strongly correlated electron system we would expect that typical relaxation times are directly related to the energy scales that appear in the spectrum, such as the bandwidth or the Mott gap. In this case all information on the initial energy ϵ is lost for pulses which are short enough to resolve the electronic dynamics. The equilibrium interpretation of conventional photoemission data in terms of the electronic spectrum of the solid thus becomes meaningless in this limit.

A full theory for time-resolved photoemission spectroscopy (TRPES), which covers both the nonequilibrium effects of the electronic state and also the consequences of the frequency uncertainty of the pulse, was

presented recently by Freericks *et al.*¹⁹ Their approach extends existing theories of conventional photoemission spectroscopy to the case where the sample is not in equilibrium and measurement pulses have a finite time duration. The photoemission intensity as a function of the probe pulse delay time is related to electronic one-particle real-time Green functions of the sample,¹⁹ which fully incorporate the nonequilibrium many-body dynamics after the pump pulse. This is in contrast to earlier Green function approaches,²⁰ which treat pump and probe on the same (perturbative) level. The relation to real-time Green functions allows to make direct contact to recent progress in nonequilibrium many-body theory, such as the extension of dynamical mean-field theory²¹ (DMFT) to nonequilibrium.^{22,23,24,25,26} DMFT, which is exact in the limit of infinite dimensions,²⁷ can provide insights into the real-time evolution of strongly correlated systems in a nonperturbative way.

The new one-particle description of TRPES given in Ref. 19 leads to the question whether real-time Green functions can be recovered fully from the time-dependent photoemission intensity, or whether parts of the electronic time evolution are not accessible by TRPES at all. Freericks *et al.* discussed the case when electronic *equilibrium states* are probed by pulses of finite time duration.^{12,19} This analysis covers experiments (e.g., those of Ref. 7) in which changes of external parameters such as the electronic temperature determine the dynamics of the electronic state, but the probe pulses are not short enough to resolve the thermalization of the electronic system in response to the pump pulse. For this case the electronic state is characterized by its frequency-dependent spectrum, and the photoemission intensity is given by this spectrum, broadened in accordance with the frequency-time uncertainty.¹⁹ Such a broadening can hamper the determination of the electronic spectrum from photoemission data; for the experiment of Ref. 7, however, it plays a minor role.¹²

By contrast, in this paper we investigate TRPES with ultrashort pulses that do resolve the thermalization of the electrons after the pump pulse. We consider systems with a purely Hamiltonian time evolution involving only electronic degrees of freedom. The electronic state is then no longer characterized only by a frequency-dependent spectrum, but rather by real-time Green functions depending on two time variables. We will show from the general theory of Ref. 19 that in this case the full time dependence on both time variables cannot be recovered from the time-dependent photoemission intensity, no matter how the pulse length of the probe pulse is chosen. While time-resolved photoemission data can be predicted from calculated nonequilibrium Green functions,¹⁹ the converse procedure is thus impossible due to the frequency-time uncertainty relation. We note that an analogous limitation is absent in time-resolved optical spectroscopy, where a two-time optical conductivity $\sigma(t, t')$ can be measured precisely by making the probe pulses sufficiently short. In nonequilibrium DMFT, $\sigma(t, t')$ is directly re-

lated to momentum-averaged real-time Green functions under certain conditions.²⁵

Below we employ the Falicov-Kimball model,²⁸ which describes localized and mobile electrons on a lattice interacting via a local Hubbard interaction, to study the relation between nonequilibrium Green functions and time-resolved photoemission data in detail. We consider an idealized setup in which the system is suddenly driven out of a metallic or insulating equilibrium state, and subsequently relaxes to a new phase due to the Hamiltonian dynamics of the electrons. This model situation was recently solved with nonequilibrium DMFT.²³ We then study hypothetical time-resolved photoemission experiments during this relaxation process, and find that some aspects of the formation of the metallic state are indeed obscured in the photoemission spectrum due to the frequency-time uncertainty. On the other hand, the relaxation of an excited Mott insulator leads to characteristic collapse-and-revival oscillations,²⁹ which result in oscillating mid-gap weight in the time-resolved photoemission spectrum. The above-mentioned uncertainty limitations notwithstanding, TRPES with ultrashort pulses is well-suited to characterize nonequilibrium states of correlated electron systems. However, it will often be necessary to analyze in detail how the time evolution of the Green function translates into the photoemission signal.

The outline of the paper is as follows. In Sec. II we briefly outline the microscopic formulation of TRPES derived in Ref. 19 and further discuss the role of the frequency-time uncertainty in this theory. We then introduce the Falicov-Kimball model (Sec. III) and discuss hypothetical time-resolved photoemission measurements on systems that relax to a metallic state (Sec. IV) and to an insulating state (Sec. V). The discussion in Sec. VI concludes the presentation.

II. TIME-RESOLVED PHOTOEMISSION SPECTROSCOPY

In photoemission experiments with both temporal and angular resolution the sample is probed with a finite pulse of definite wave vector³⁰ \mathbf{q} . The detector collects the photoelectrons which are emitted in a certain direction $\hat{\mathbf{k}}_e$, and it is sensitive to their kinetic energy $E = \hbar^2 k_e^2 / 2m$, but not to their arrival time ($\mathbf{k}_e = \hat{\mathbf{k}}_e k_e$ is the photoelectron momentum). The time-resolved photoemission signal is thus proportional to the total number of electrons per solid angle $d\Omega_{\hat{\mathbf{k}}_e}$ and energy interval dE

$$I(\hat{\mathbf{k}}_e, E; \mathbf{q}, t_p) = \frac{dN(\hat{\mathbf{k}}_e, E; \mathbf{q}, t_p)}{d\Omega_{\hat{\mathbf{k}}_e} dE} \quad (1)$$

that are emitted in response to a pulse that hits the sample at time t_p .¹⁹ This definition includes only photoelectrons excited by the probe pulse and omits direct photoemission due to the pump pulse.

In Ref. 19 an expression for the photoemission signal (1) was derived, using only the so-called sudden approximation,³¹ which neglects the interaction of photoelectrons with the remaining sample. The photoemission signal is then only related to matrix elements $M(\mathbf{k}, \mathbf{q}; \mathbf{k}_e)$ which couple Bloch states with quasi-momentum \mathbf{k} in the solid and one-electron scattering states with asymptotic momentum \mathbf{k}_e via absorption of a photon with momentum \mathbf{q} , and to the real-time one-particle Green function

$$G_{\mathbf{k}, \mathbf{k}'}^<(t, t') = i \text{Tr}[\rho_0 c_{\mathbf{k}'}^\dagger(t') c_{\mathbf{k}}(t)]. \quad (2)$$

The latter incorporates the full nonequilibrium dynamics of the sample: $c_{\mathbf{k}}^{(\dagger)}(t) = U(t, t_{\min})^\dagger c_{\mathbf{k}}^{(\dagger)} U(t, t_{\min})$ are annihilation (creation) operators for electrons in the solid with momentum \mathbf{k} , whose propagation in time, with $U(t, t_{\min}) = T_\tau \exp[-i \int_{t_{\min}}^t d\tau H(\tau)/\hbar]$, includes all external fields except for the probe. The initial state at some early time t_{\min} is usually given by the thermal ensemble at temperature T , $\rho_0 \propto \exp[-H(t_{\min})/T]$. The presence of the surface and the dependence of photoemission spectra on matrix elements can substantially complicate the comparison of theoretical and experimental data for specific materials. In order to reveal general aspects of TRPES we thus resort to further approximations that are commonly made in this context: (i) We assume that photoemission measures the bulk properties of the sample which are contained in the momentum-diagonal Green function $G_{\mathbf{k}}^<(t, t') \equiv G_{\mathbf{k}\mathbf{k}}^<(t, t')$ of the infinite and translationally invariant system, and (ii), we take matrix elements to be constant but satisfying momentum conservation in the plane, $M(\mathbf{q}, \mathbf{k}; \mathbf{k}_e) \equiv M \delta_{\mathbf{k}_{\parallel} + \mathbf{q}_{\parallel}, \mathbf{k}_{e\parallel}}$. The time-resolved photoemission spectrum (1) is then given by¹⁹

$$I(\hat{\mathbf{k}}_e, E; \mathbf{q}, t_p) \propto \sum_{\mathbf{k}\sigma} \delta_{\mathbf{k}_{\parallel} + \mathbf{q}_{\parallel}, \mathbf{k}_{e\parallel}} \mathcal{I}_{\mathbf{k}\sigma}(E - c\mathbf{q} - \Phi; t_p), \quad (3)$$

$$\begin{aligned} \mathcal{I}_{\mathbf{k}\sigma}(\omega; t_p) &= -i \int dt \int dt' S(t) S(t') \\ &\times e^{i\omega(t'-t)} G_{\mathbf{k}\sigma}^<(t + t_p, t' + t_p), \end{aligned} \quad (4)$$

where $S(\tau)$ is the (real) pulse envelope function (centered at $\tau = 0$) and Φ is the work function of the solid. Note that Eqn. (3) and (4) become exact for perfectly layered (two-dimensional) structures, when \mathbf{k} denotes the two-dimensional momentum of the sample. In the following we will discuss the momentum- and frequency-dependent expression (4). For simplicity we will refer to Eq. (4) as the photoemission intensity; observations made for this function presumably persist after summation over some part of the Brillouin zone [Eq. (3)].

Eq. (4) simplifies when the system is in equilibrium. In this case Green functions depend on the time difference only, and the Fourier transform is given by³²

$$g_{\mathbf{k}\sigma}^<(\omega) = \int dt e^{i\omega t} G_{\mathbf{k}\sigma}^<(t, 0) = 2\pi i A_{\mathbf{k}\sigma}(\omega) f(\omega), \quad (5)$$

where $A_{\mathbf{k}\sigma}(\omega)$ is the equilibrium spectral function,³² and $f(\omega) = 1/(e^{\omega/T} + 1)$ is the Fermi function for temperature T . The photoemission intensity then reduces to

$$\mathcal{I}_{\mathbf{k}\sigma}(\omega) = \int d\omega' |\tilde{S}(\omega + \omega')|^2 A_{\mathbf{k}\sigma}(\omega') f(\omega'), \quad (6)$$

which is a convolution of the well-known expression $\mathcal{I}_{\mathbf{k}\sigma}(\omega) \propto A_{\mathbf{k}\sigma}(\omega) f(\omega)$ for the intrinsic photocurrent in continuous beam experiments^{17,18} with the Fourier transform $\tilde{S}(\omega) = \int dt S(t) e^{i\omega t}$ of the pulse envelope. Due to the frequency-time uncertainty of the pulse, the frequency-dependent spectrum is thus smoothed on a scale $\delta\omega > 1/\delta t$ when the pulse has a finite length δt , as discussed in Refs. 19 and 12.

Here we study the case of an electronic system that is not in equilibrium. The Green function $G_{\mathbf{k}\sigma}^<(t, t + s)$ then contains important information both in the absolute time t and in the time difference s between addition and removal of an electron. However, when the probe pulse extends only over a finite length δ , the product $S(t)S(t')$ in Eq. (4) vanishes for all $t - t' > \delta$, and hence $G_{\mathbf{k}\sigma}^<(t, t + s)$ enters Eq. (4) only for $s < \delta$. It is therefore impossible to deduce $G_{\mathbf{k}\sigma}^<(t, t + s)$ from spectra that were recorded with pulses of length $\delta < s$. In other words, the time resolution (in t) with which $G_{\mathbf{k}\sigma}^<(t, t + s)$ can be measured is limited by s . This also becomes clear when attempting to invert the convolution of $G_{\mathbf{k}\sigma}^<(t, t')$ in Eq. (4): Starting from the Fourier transform

$$\tilde{\mathcal{I}}_{\mathbf{k}\sigma}(s; t_p) = \int d\omega e^{i\omega s} \mathcal{I}_{\mathbf{k}\sigma}(\omega; t_p), \quad (7)$$

and using, e.g., Gaussian pulses,

$$S(t) = \exp\left(-\frac{t^2}{2\delta^2}\right), \quad (8)$$

we obtain

$$\begin{aligned} \tilde{\mathcal{I}}_{\mathbf{k}\sigma}(s; t_p) &\propto \exp\left(-\frac{s^2}{4\delta^2}\right) \\ &\times \int dt G_{\mathbf{k}\sigma}^<\left(t_p + \frac{s}{2} + t, t_p - \frac{s}{2} + t\right) \exp\left(-\frac{t^2}{\delta^2}\right). \end{aligned} \quad (9)$$

While the integral in (9) apparently measures $G_{\mathbf{k}\sigma}^<(t_p + s/2, t_p - s/2)$ with a time resolution of δ , it is practically impossible to choose $\delta \ll s$ because then the result vanishes compared to any noise added to $\tilde{\mathcal{I}}_{\mathbf{k}\sigma}(s; t_p)$, due to the Gaussian prefactor (whose form is due to (8) but the suppression of the signal for $\delta \ll s$ is independent of the pulse shape). We conclude that the nonequilibrium two-time Green function cannot be fully measured by means of TRPES, and one must always carefully analyze how the time evolution of the Green function translates into the photoemission signal for a given theoretical model. This will be illustrated for the Falicov-Kimball model below.

III. THE FALICOV-KIMBALL MODEL IN NONEQUILIBRIUM

In the remaining part of this paper we concentrate on one specific model for electronic dynamics in a single band, the Falicov-Kimball model.²⁸ This lattice model describes itinerant (\downarrow) and immobile (\uparrow) electrons which interact via the local Coulomb repulsion U . The Hamiltonian is given by

$$H = \sum_{ij} V_{ij} c_{i\downarrow}^\dagger c_{j\downarrow} + U \sum_i n_{i\downarrow} n_{i\uparrow} - \sum_{i\sigma} \mu_\sigma n_{i\sigma}, \quad (10)$$

where $c_{i\sigma}^{(\dagger)}$ are annihilation (creation) operators for the two species of fermions on lattice site i , and $n_{i\sigma} = c_{i\sigma}^\dagger c_{i\sigma}$ is the corresponding density ($\sigma = \downarrow, \uparrow$). Hopping between sites i and j (with amplitude V_{ij}) is possible only for the mobile (\downarrow) particles. The Falicov-Kimball model has been an important benchmark for the development of DMFT in equilibrium, because the effective single-site problem for the mobile particles is quadratic and can be solved exactly.³³ This model currently plays a similar role for nonequilibrium DMFT,^{22,23,24,25,26} in particular since no appropriate real-time impurity solver is yet available for the Hubbard model.

In spite of its apparent simplicity the Falicov-Kimball model has a rich equilibrium phase diagram containing metallic, insulating, and charge-ordered phases.³⁴ In the following we consider only the homogeneous phase at half-filling for both particle species ($n_\downarrow = n_\uparrow = 1/2$), which in equilibrium undergoes a metal-insulator transition at a critical interaction $U = U_c$ on the order of the bandwidth.^{33,34,35,36} This phase is studied in an idealized nonequilibrium situation, by preparing the system in thermal equilibrium for times $t < 0$, and changing the interaction parameter U abruptly at $t = 0$.²³ Of course within a more realistic description of the pump pulse the system would not be excited into a state that is an equilibrium state of any simple Hamiltonian. Nonetheless, the *interaction quench* we study here allows us to discuss time-resolved photoemission signals for a situation in which the electronic dynamics drives the system between different phases. Since the exact DMFT solution for the interaction quench is available²³ we can directly relate Green functions and photoemission signals. In particular, we will focus on two specific phenomena, namely (i) the formation of narrow quasiparticle resonances during the buildup of the metallic state (Sec. IV), and (ii) coherent collective oscillations after an excitation of the insulating phase (Sec. V).

In the following we analyze the time-resolved photoemission signal of the mobile (\downarrow) electrons using Gaussian pulses (8) and omit the time-independent contribution of the immobile (\uparrow) electrons. As in Ref. 23 we assume a semielliptic density of states $\rho(\epsilon) = \sqrt{4V^2 - \epsilon^2}/(2\pi V^2)$ with half-bandwidth $2V$ for the single-particle energies $\epsilon_{\mathbf{k}}$, which are the eigenvalues of the hopping matrix V_{ij} . Exact expressions for the real-time Green func-

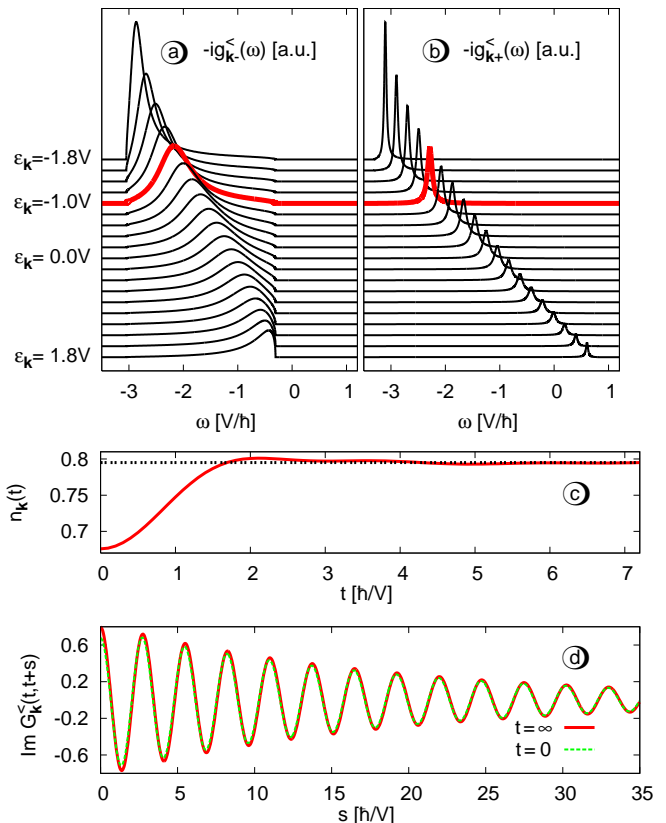


FIG. 1: The momentum-dependent Green function $g_{\mathbf{k}\pm}^<(\omega)$ [Eq. (11)] in the initial (a) and final (b) state for the quench from $U = 3$ to $U = 0.5$ ($n_c = n_f = 1/2$; temperature $T = 0$). Due to the local self-energy in DMFT, $G_{\mathbf{k}}^<(t, t')$ depends on \mathbf{k} only via $\epsilon_{\mathbf{k}}$ in the homogeneous phase. (c) Density $n_{\mathbf{k}}(t)$ for momentum \mathbf{k} with $\epsilon_{\mathbf{k}} = -1$ [thick red curve in (a) and (b)]. The horizontal line is at $n_{\mathbf{k}}(\infty)$. (d) Green function $G_{\mathbf{k}}^<(t + s, t)$ for the same $\epsilon_{\mathbf{k}}$. Differences between the Green functions for $t = 0$ and $t = \infty$ are best visible around $s = 0$; their decay is almost identical.

tions $G_{\mathbf{k}}^<(t, t')$ of the mobile electrons are given in the Appendix (from now on we suppress the index \downarrow of the mobile electrons). We take $V = 1$ as the unit of energy, so that the full bandwidth is 4 and the critical interaction is given by $U_c = 2V = 2$.³⁶ We will also set $\hbar = 1$, setting the unit of time as \hbar/V . For example, for $V = 1$ eV we have $\hbar/V = 0.66$ fs.

IV. PUMPING THE INSULATOR INTO A METALLIC STATE

In this section we investigate the formation of a metallic state in real time, similar to pump-induced insulator-to-metal transitions on ultrashort time scales.^{4,5,7,8} In the Falicov-Kimball model, such a process takes place after a quench from an insulating state to the metallic parameter regime, which we consider now. We prepare the initial

state at $U = 3$ and temperature $T = 0$, and change the interaction abruptly to $U = 0.5$ at time $t = 0$. Subsequently the system relaxes to a new stationary state, in which Green functions depend on time difference only.²³ In the following we first discuss the real-time Green functions for this process and then the corresponding time-resolved photoemission signal.

A. Real-time Green functions

The difference between the initial and final state is evident from the momentum-diagonal Green function $G_{\mathbf{k}}^<(t, t')$ of the mobile particles [Eq. (2)] and its Fourier transform

$$g_{\mathbf{k}\mp}^<(\omega) \equiv \lim_{t \rightarrow \mp\infty} \int ds e^{i\omega s} G_{\mathbf{k}}^<(t+s, t) \quad (11)$$

in the limit $t = \mp\infty$, respectively: While $g_{\mathbf{k}-}^<(\omega)$ has a broad maximum (Fig. 1a), a sharp peak in $g_{\mathbf{k}+}^<(\omega)$ indicates that quasiparticle excitations have a long lifetime in the final state (Fig. 1b). Note that for a quench in the Falicov-Kimball model the final state always retains memory on the initial configuration.²³ This memory is contained in a nonuniversal occupation function $F(\omega)$ which replaces the Fermi function $f(\omega)$ in Eq. (5), i.e., $g_{\mathbf{k}+}^<(\omega) = 2\pi i A_{\mathbf{k}}(\omega) F(\omega)$ (see Appendix).

The development of the metallic state with its sharp quasiparticle-like resonances can be observed from the full time dependence of the momentum-diagonal Green function $G_{\mathbf{k}}^<(t, t')$. In particular, we characterize the transition by means of (i) the total spectral weight, i.e., the momentum occupation $n_{\mathbf{k}}(t) = -iG_{\mathbf{k}}^<(t, t)$, and (ii) the decay of $G_{\mathbf{k}}^<(t, t+s)$ as a function of $s > 0$. From the latter one can read off the lifetime of a hole which is created at time t in the nonequilibrium state. The time evolution of these two quantities is similar for all \mathbf{k} ; it is shown for one representative value of \mathbf{k} in Fig. 1c and 1d (namely $\epsilon_{\mathbf{k}} = -1$, marked by the thick red line in Fig. 1a and 1b): (i) Relaxation of the momentum occupation $n_{\mathbf{k}}(t)$ takes place on a time scale on the order of the inverse bandwidth; after this very short time interval the final value $n_{\mathbf{k}}(\infty)$ is almost reached, and a slower relaxation follows (Fig. 1c). A similar behavior was observed previously for the time dependence of the number of doubly occupied sites.²³ (ii) As a function of s , the Green function $G_{\mathbf{k}}^<(t, t+s)$ decays slow compared to the inverse bandwidth (Fig. 1d). For $t = \infty$, this is in accordance with the sharp peak in $g_{\mathbf{k}+}^<(\omega)$. However, the fast decay is observed even for holes that are created at $t = 0^+$, when the system is still in the insulating state, indicating that the lifetime of hole excitations depends only weakly on the time of their creation. The reason for this behavior is that in the Falicov-Kimball model scattering occurs only between mobile and immobile particles and is thus determined by the Hamiltonian and the (initial) configuration of the immobile particles. If scattering occurred between two mobile electron species (e.g., as in

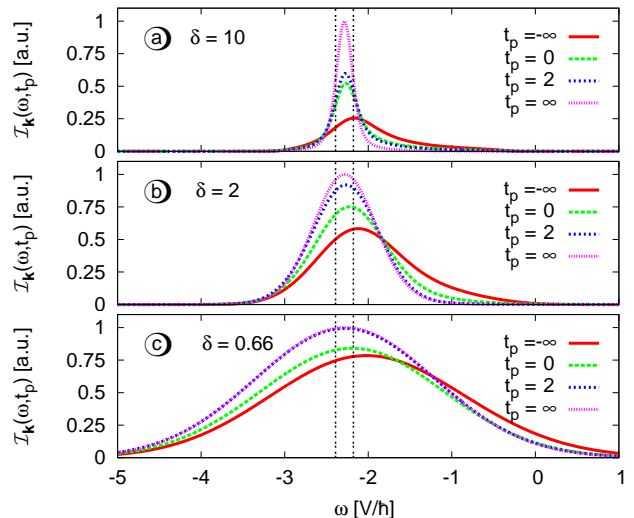


FIG. 2: Photoemission signal [Eq. (4)] (a.u.) for the same situation as the Green functions in Fig. 1 ($\epsilon_{\mathbf{k}} = -1$), using Gaussian probe envelopes (8) with $\delta = 10$ (a), $\delta = 2$ (b), and $\delta = 0.66$ (c). The vertical dashed lines are explained in the text. t_p and δ are in units of $\hbar/V = 1$.

the Hubbard model), then we would expect the shape of the quasiparticle resonances to depend on the quantum state of the mobile particles as well, and therefore would expect it to change considerably during the relaxation process.

B. Photoemission spectrum

As discussed in the introduction, it is a central question whether the time-resolved photoemission spectrum $\mathcal{I}_{\mathbf{k}}(\omega; t_p)$ [Eq. (4)] contains the same information as the Green function $G_{\mathbf{k}}^<(t, t')$. For the present case, the answer is no: In the last subsection we saw that holes decay at a rate $\Gamma \ll V/\hbar$, which depends only weakly on the time t when the hole is created, even for short times $0 < t < \hbar/V$. To establish this behavior from the photoemission intensity, however, one would have to measure $G_{\mathbf{k}}(t, t+1/\Gamma)$ with time resolution better than \hbar/V , which is impossible according to the discussion at the end of Sec. II.

The effect of the frequency-time uncertainty can be seen in detail in the redistribution of spectral weight in the photoemission signal $\mathcal{I}_{\mathbf{k}}(\omega; t_p)$ as a function of the probe time t_p (for $\epsilon_{\mathbf{k}} = -1$, Fig. 2). When the system is probed in a stationary state ($t_p = \pm\infty$), the intensity is given by $g_{\mathbf{k}\pm}^<(\omega)$ folded with the spectrum $|\hat{S}(\omega)|^2 = 2\pi\delta^2 \exp(-\delta^2\omega^2)$ of the probe pulse [cf. Eq. (6)]. This broadening completely washes out the peak for short pulses ($\delta = 0.66$ in units of \hbar/V , Fig. 2c). On the other hand, pulses much longer than the inverse bandwidth do not resolve the fast relaxation which is essentially com-

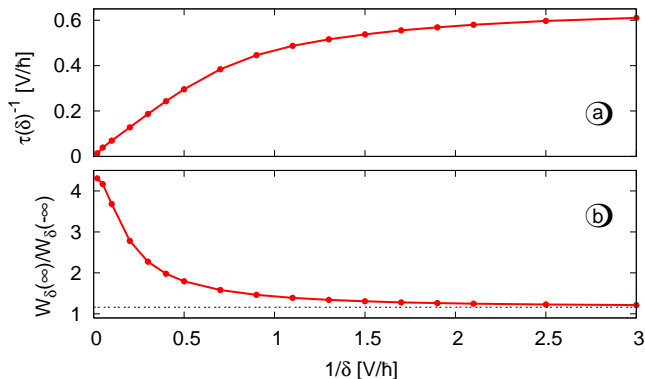


FIG. 3: (a) Relaxation time $\tau(\delta)$ [Eq. (13), $\eta = 0.95$] for the spectral width in the central peak region of the photoemission spectrum at $\epsilon_{\mathbf{k}} = -1$ (region between the vertical dashed lines in Fig. 2), plotted against the pulse length δ . (b) Ratio $W_\delta(\infty)/W_\delta(-\infty)$. The horizontal dashed line is at $n_{\mathbf{k}}(\infty)/n_{\mathbf{k}}(-\infty)$.

plete for $t > 2$, but rather show a time dependence even for $t \gtrsim 2$ ($\delta = 10$, Fig. 2a). For intermediate pulse length neither time nor frequency dependence is resolved ($\delta = 2$, Fig. 2b).

For a quantitative analysis we now consider the weight in the central region of the peak in the photoemission spectrum,

$$W_\delta(t_p) \equiv \int_a^b d\omega \mathcal{I}_{\mathbf{k}}(\omega; t_p). \quad (12)$$

In the present case we use $a = -2.39$ and $b = -2.17$ as indicated by the vertical dashed lines in Fig. 2; they enclose twice the full width at half maximum of a Lorentzian fit to the peak in $A_{\mathbf{k}}(\omega)$. We then define a time $\tau(\delta)$ at which the relaxation of $W_\delta(t_p)$ is essentially complete,

$$\frac{W_\delta[\tau(\delta)] - W_\delta(-\infty)}{W_\delta(\infty) - W_\delta(-\infty)} = \eta, \quad (13)$$

with η close to one; we use $\eta = 0.95$. In Fig. 3a we see first of all that $\tau(\delta)$ is proportional to the pulse length for large δ , which is due to the fact that long pulses merely average the spectrum of the final and initial state. Hence $\tau(\delta)$ does not yield any information about intrinsic relaxation times for $\delta \gtrsim 2$. On the other hand, for $\delta \lesssim 2$ the ratio $W_\delta(\infty)/W_\delta(-\infty)$ approaches the value $n_{\mathbf{k}}(\infty)/n_{\mathbf{k}}(-\infty)$ that one would obtain by integrating over the whole spectrum instead of the peak region alone (Fig. 3b); this is due to the insufficient energy resolution. Therefore only the relaxation time of the whole spectral width, i.e., of the momentum occupation $n_{\mathbf{k}}(t)$, can be determined reliably.

V. OSCILLATIONS OF AN EXCITED MOTT INSULATOR

In this section we investigate the relaxation dynamics of a Mott insulator in which a metallic state has been created by the pump pulse. In the Falicov-Kimball model this can be simulated in the strongly interacting regime ($U = 10$) by preparing the system in a metallic state ($U = 1$, temperature $T = 0$) at $t = 0$. Again we first discuss the real-time Green functions for this situation and then the time-resolved photoemission signal that corresponds to them.

A. Real-time Green functions

In the present case the momentum-dependent Green function evolves from a well-defined quasiparticle band at $t = -\infty$, which is cut off by the Fermi function (Fig. 4a), to a gapped spectrum at $t = \infty$ (Fig. 4b). Note that in the final state spectral weight remains in the upper band because the system is strongly excited with respect to the insulating ground state at $U = 10$, and there is no coupling to an environment to which this excess energy could be passed during the relaxation process.

As in the previous section we consider a representative momentum ($\epsilon_{\mathbf{k}} = 1$), chosen such that $n_{\mathbf{k}}$ is small in the metallic state and increases after the quench (Fig. 4c). Again this relaxation takes place on a very short time scale (on the order of the inverse bandwidth), but now $n_{\mathbf{k}}$ passes through a series of damped oscillations with period $2\pi/U$ before reaching its final value. These oscillations are characteristic for the dynamics of a Mott insulator which is dominated by a Hubbard-type density interaction $U \sum_i n_{i\uparrow} n_{i\downarrow}$. In fact, if the Hamiltonian were given only by this interaction term, then the time evolution operator $\exp(-itU \sum_i n_{i\uparrow} n_{i\downarrow})$ would itself be $2\pi/U$ -periodic,²⁹ and hence oscillations would occur in all nonlocal quantities. These so-called collapse-and-revival oscillations were first observed and described in experiments with ultracold atomic gases,²⁹ where the Hamiltonian of the system can be designed in a controlled way. We will now discuss the fingerprint of these oscillations in the time-resolved photoemission spectrum.

B. Photoemission spectrum

In Fig. 5 the angular-resolved photoemission spectrum $\mathcal{I}_{\mathbf{k}}(\omega; t_p)$ is plotted for the same fixed momentum [$\epsilon_{\mathbf{k}} = 1$, using Gaussian pulses (8)]. All features of the spectrum except for its total weight, which is proportional to $n_{\mathbf{k}}(t)$, are washed out for short pulses ($\delta = 0.2$, Fig. 5c), whereas long pulses show the formation of a gap, but cannot resolve the oscillating nature of the state ($\delta = 0.66$, Fig. 5a). For intermediate pulses, however, both the $2\pi/U$ -periodicity and the gap become visible ($\delta = 0.33$, Fig. 5b).

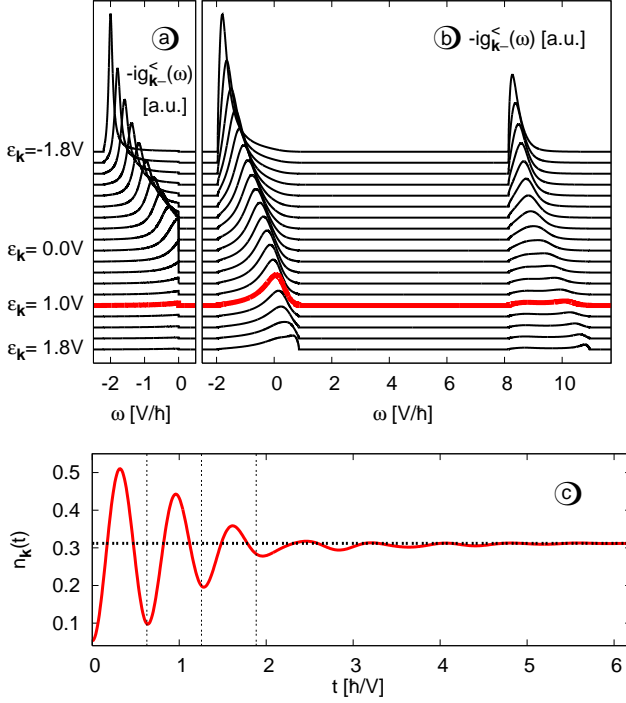


FIG. 4: The momentum-dependent Green function $g_{\mathbf{k}\pm}^<(\omega)$ [Eq. (11)] in the initial (a) and final (b) state for the quench from $U = 1$ to $U = 10$ ($n_c = n_f = 1/2$; temperature $T = 0$). (c) Density $n_{\mathbf{k}}(t)$ for momentum \mathbf{k} with $\epsilon_{\mathbf{k}} = 1$ [thick red curve in (a) and (b)]. The vertical dashed lines are at multiples of the fundamental oscillation period $2\pi/U$. The horizontal line is $n_{\mathbf{k}}(\infty)$.

Interestingly, the coherent oscillations are most pronounced in the center of the gap (Fig. 5b). This observation can be understood from the atomic limit of the Hamiltonian (10), i.e., for $V_{ij} = 0$. In the strongly interacting regime $U \gg V$ the atomic limit gives a good description of the transient behavior at short times $t \lesssim \hbar/V$. For the interaction term alone, $H_U = U \sum_i n_{i\uparrow} n_{i\downarrow} - \sum_{i\sigma} \mu_{\sigma} n_{i\sigma}$ the time evolution of annihilation operators is given by $e^{iH_U t} c_{j\sigma} e^{-iH_U t} = e^{i\mu_{\sigma} t} [c_{j\sigma} + (e^{-itU} - 1)c_{j\sigma} n_{i\bar{\sigma}}]$. For $t, t' > 0$, the Green function then follows as

$$G_{\mathbf{k}\sigma}^<(t, t') = ie^{i\mu_{\sigma}(t-t')} [A_{\mathbf{k}\sigma} + B_{\mathbf{k}\sigma} e^{it'U} + B_{\mathbf{k}\sigma}^* e^{-itU} + C_{\mathbf{k}\sigma} e^{iU(t'-t)}], \quad (14a)$$

with

$$A_{\mathbf{k}\sigma} = \sum_{ij} e^{i\mathbf{k}(\mathbf{R}_i - \mathbf{R}_j)} \langle (1 - n_{j\bar{\sigma}}) c_{j\sigma}^{\dagger} c_{i\sigma} (1 - n_{i\bar{\sigma}}) \rangle_0 \quad (14b)$$

$$B_{\mathbf{k}\sigma} = \sum_{ij} e^{i\mathbf{k}(\mathbf{R}_i - \mathbf{R}_j)} \langle n_{j\bar{\sigma}} c_{j\sigma}^{\dagger} c_{i\sigma} \rangle_0 \quad (14c)$$

$$C_{\mathbf{k}\sigma} = \sum_{ij} e^{i\mathbf{k}(\mathbf{R}_i - \mathbf{R}_j)} \langle n_{j\bar{\sigma}} c_{j\sigma}^{\dagger} c_{i\sigma} n_{i\bar{\sigma}} \rangle_0, \quad (14d)$$

and $\langle \cdot \rangle_0$ is the expectation value in the (arbitrary) state

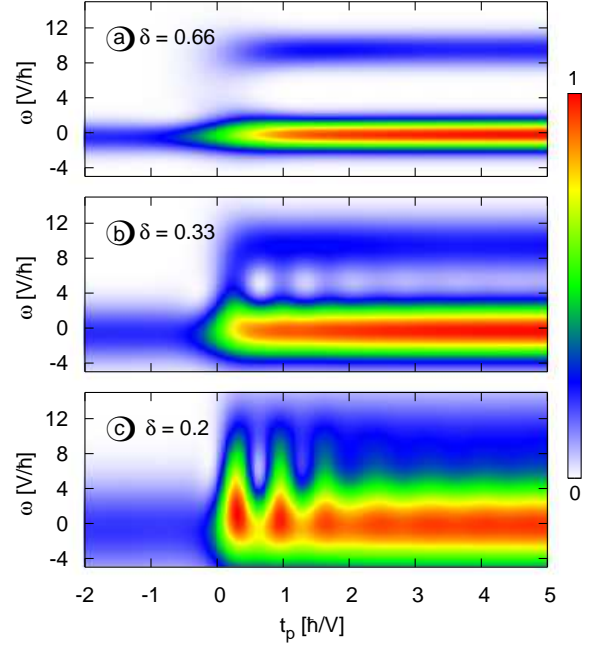


FIG. 5: Quench from $U = 1$ to $U = 10$: Photoemission signal (a.u.) [Eq. (4)] for $\epsilon_{\mathbf{k}} = 1$, and Gaussian probe envelopes (8) with $\delta = 0.66$ (a), $\delta = 0.33$ (b), and $\delta = 0.2$ (c). Pulse lengths δ are in units of $\hbar/V = 1$.

at $t = 0$ immediately after the pump. Inserting this expression into Eq. (4) we find, for $t_p \gg \delta$,

$$\mathcal{I}_{\mathbf{k}\sigma}(\omega; t_p) \propto A_{\mathbf{k}\sigma} |\tilde{S}(\omega + \mu_{\sigma})|^2 + C_{\mathbf{k}\sigma} |\tilde{S}(\omega + \mu_{\sigma} - U)|^2 + 2 \text{Re}[\tilde{S}(\omega) \tilde{S}(\omega + \mu_{\sigma} - U) B_{\mathbf{k}\sigma} e^{it_p U}]. \quad (15)$$

The first two terms are centered in the upper and lower Hubbard bands at $\omega = -\mu_{\sigma}$ and $\omega = U - \mu_{\sigma}$ and do not change with time. The third term, which oscillates with period $2\pi/U$, has its maximum where $\tilde{S}(\omega + \mu_{\sigma})$ and $\tilde{S}(\omega + \mu_{\sigma} - U)$ overlap. For Gaussian pulses, this is precisely the center of the gap because $\tilde{S}(\omega) \tilde{S}(\omega - U) \propto e^{-(\omega - U/2)^2 / 2\delta^2} e^{-U^2 / \delta^2}$.

This discussion shows that on short time scales the observed time-dependent spectrum in the Falicov-Kimball model for large interactions resembled that of the atomic limit. Note that the initial state at $t = 0$ determines only the weight of the three components, but not the frequency of the oscillations. The oscillating midgap weight is thus a universal property of the Mott insulator, which is largely independent of the excitation process. Via this universal feature it may eventually become possible to observe collapse-and-revival oscillations in TRPES experiments on correlated materials.

VI. CONCLUSION

In this paper we analyzed hypothetical time-resolved photoemission experiments on correlated electron sys-

tems that are not in equilibrium, building on the general theory of Ref. 19. We showed that the two-time Green function, which characterizes the nonequilibrium state of the electrons, cannot be fully measured with TRPES, no matter how long or short the probe pulses are chosen. For example, using DMFT for the Falicov-Kimball model we found that in the buildup of the metallic state the Green function of the transient state cannot be determined from the photoemission signal. On the other hand, if an excited Mott insulator is created by the pump pulse, its characteristic collapse-and-revival oscillations can nevertheless be inferred because they correspond to oscillating weight in the center of the Mott gap in the time-dependent photoemission spectrum.

TRPES is in some sense complementary to time-resolved optical spectroscopy, which measures the two-time optical conductivity $\sigma(t, t')$. Under certain conditions, the latter is obtained in DMFT from a momentum-averaged product of two Green functions that also enter the expression for the photoemission spectrum.²⁵ The dependence of $\sigma(t, t')$ on both t and t' can be measured precisely with sufficiently short probe pulses, unaffected by any minimum uncertainty, but unlike in photoemission spectroscopy there is no sensitivity toward specific momenta \mathbf{k} .

In conclusion, we showed that in spite of the frequency-time uncertainty of the probe pulse, TRPES has the potential to discover fascinating details of the electronic thermalization process. Unlike for conventional photoemission on systems in equilibrium, however, the time-dependent photoemission signal does not yield the real-time Green function directly, so that more detailed comparisons to theoretical predictions are needed.

Acknowledgements

We thank Dieter Vollhardt for valuable discussions. M.E. acknowledges support by Studienstiftung des Deutschen Volkes. This work was supported in part by the SFB 484 of the Deutsche Forschungsgemeinschaft.

APPENDIX A: CALCULATION OF DMFT GREEN FUNCTIONS

1. Contour Green functions

In this appendix, which is a direct extension of the work presented in Ref. 23, we give the detailed derivation of the real-time Green functions for the interaction quench in the Falicov-Kimball model, using DMFT for nonequilibrium.²²

The retarded, advanced, and lesser Green functions are

defined by

$$G_{\mathbf{k}\sigma}^r(t, t') = -i\Theta(t - t')\text{Tr}[\rho_0\{c_{\mathbf{k}\sigma}(t), c_{\mathbf{k}\sigma}^\dagger(t')\}] \quad (\text{A1a})$$

$$G_{\mathbf{k}\sigma}^a(t, t') = i\Theta(t' - t)\text{Tr}[\rho_0\{c_{\mathbf{k}\sigma}(t), c_{\mathbf{k}\sigma}^\dagger(t')\}] \quad (\text{A1b})$$

$$G_{\mathbf{k}\sigma}^<(t, t') = i\text{Tr}[\rho_0 c_{\mathbf{k}\sigma}^\dagger(t')c_{\mathbf{k}\sigma}(t)] \quad (\text{A1c})$$

respectively, where $c_{\mathbf{k}\sigma}(t)$ and ρ_0 are defined below Eq. (2). DMFT for nonequilibrium is based on the Keldysh formalism,^{37,38} which yields the contour-ordered Green function $G_{\mathbf{k}\sigma}(t, t') = -i\langle T_{\mathcal{C}}c_{\mathbf{k}\sigma}(t)c_{\mathbf{k}\sigma}^\dagger(t') \rangle$ with time arguments on the contour \mathcal{C} that runs from t_{\min} to t_{\max} on the real axis, then from t_{\max} to t_{\min} , and finally to $t_{\min} - i\beta$ on the imaginary time axis (β : inverse temperature). Retarded, advanced, and lesser Green functions (A1) are obtained from the real-time components of the contour Green function,³⁸

$$G_{\mathbf{k}\sigma}^r(t, t') = [G_{\mathbf{k}\sigma}^{11}(t, t') - G_{\mathbf{k}\sigma}^{12}(t, t')] \quad (\text{A2a})$$

$$G_{\mathbf{k}\sigma}^a(t, t') = [G_{\mathbf{k}\sigma}^{11}(t, t') - G_{\mathbf{k}\sigma}^{21}(t, t')] \quad (\text{A2b})$$

$$G_{\mathbf{k}\sigma}^<(t, t') = G_{\mathbf{k}\sigma}^{12}(t, t'), \quad (\text{A2c})$$

where superscripts refer to the two time arguments: 1, 2, and 3 indicates whether a time argument is on the upper, lower, or vertical part of the contour, respectively. These relations and also the symmetries

$$G_{\mathbf{k}\sigma}^r(t, t') = G_{\mathbf{k}\sigma}^a(t', t)^* \quad (\text{A3a})$$

$$G_{\mathbf{k}\sigma}^<(t, t') = -G_{\mathbf{k}\sigma}^<(t', t)^* \quad (\text{A3b})$$

hold for all contour Green functions considered here. Furthermore, the contour Green functions obey antiperiodic boundary conditions in both contour arguments:

$$G_{\mathbf{k}\sigma}^{\nu 1}(t, t_{\min}) = -G_{\mathbf{k}\sigma}^{\nu 3}(t, t_{\min} - i\beta), \quad (\text{A4a})$$

$$G_{\mathbf{k}\sigma}^{1\nu}(t_{\min}, t') = -G_{\mathbf{k}\sigma}^{3\nu}(t_{\min} - i\beta, t'), \quad (\text{A4b})$$

for $\nu = 1, 2, 3$.

For the lattice Hamiltonian (10), the interacting contour Green function satisfies a Dyson equation³⁸

$$[(\mathcal{G}_{\mathbf{k}\sigma}^{-1} - \Sigma_{\mathbf{k}\sigma}) * G_{\mathbf{k}\sigma}](t, t') = \delta^{\mathcal{C}}(t, t'), \quad (\text{A5a})$$

where $\Sigma_{\mathbf{k}\sigma}(t, t')$ is the contour self-energy, and $\mathcal{G}_{\mathbf{k}\sigma}(t, t')$ is the noninteracting Green function, whose inverse

$$\mathcal{G}_{\mathbf{k}\sigma}^{-1}(t, t') = \delta^{\mathcal{C}}(t, t')[(i\partial_t^{\mathcal{C}} + \mu_{\sigma}) - \epsilon_{\mathbf{k}\sigma}(t)] \quad (\text{A5b})$$

can be written as differential operator on the contour. Here we assumed a homogeneous state, and $\epsilon_{\mathbf{k}\sigma} = \sum_j V_{ij}^{\sigma} \exp[i\mathbf{k}(\mathbf{R}_j - \mathbf{R}_i)]$ are the single-particle band energies. We also introduced the convolution $(f * g)(t, t') = \int_{\mathcal{C}} d\bar{t} f(t, \bar{t})g(\bar{t}, t')$ of two functions along the contour, the contour delta function $\delta^{\mathcal{C}}(t, t')$ [defined by $\int_{\mathcal{C}} d\bar{t} f(\bar{t})\delta^{\mathcal{C}}(\bar{t}, t) = f(t)$], and the contour derivative $\partial_t^{\mathcal{C}}$.²² Taking into account the boundary conditions (A4), the integro-differential equation (A5) has a unique solution for $G_{\mathbf{k}\sigma}(t, t')$.

2. DMFT equations

In DMFT the self-energy is assumed to be local in space, and hence independent of \mathbf{k} for a homogeneous state. This approximation is exact in the limit of infinite spatial dimensions,²⁷ both for equilibrium and for the Keldysh self-energy.²² The local self-energy $\Sigma_\sigma(t, t')$ and the local Green function $G_\sigma(t, t') \equiv G_{ii\sigma}(t, t') = \sum_{\mathbf{k}} G_{\mathbf{k}\sigma}(t, t')$ are then calculated from an auxiliary problem in which the degrees of freedom at a single lattice site i are coupled to some unknown environment, which must be determined self-consistently. For the Falicov-Kimball model, the auxiliary problem is quadratic^{22,33} such that the equations of motion can be solved explicitly.

The DMFT equations for the interaction quench in the Falicov-Kimball model were derived in Ref. 23. In the following we state these equations without derivation, and then give details of the solution. In particular we calculate the momentum-dependent Green function $G_{\mathbf{k}}(t, t') \equiv G_{\mathbf{k}\downarrow}(t, t')$ of the mobile (\downarrow) particles, which is needed for the photoemission intensity (4). From now on we consider only properties of the mobile particles, and omit the index \downarrow .

The local Green function of the mobile particles is given by the sum

$$G(t, t') = w_0 Q(t, t') + w_1 R(t, t'), \quad (\text{A6a})$$

of the local Green functions $Q(t, t')$ and $R(t, t')$ at sites with zero and one immobile (\uparrow) particle, respectively, weighted with the average density $w_1 = 1 - w_0$ of immobile particles. The functions $Q(t, t')$ and $R(t, t')$ obey the equations of motion

$$[i\partial_t^{\mathcal{C}} + \mu]Q(t, t') - (\Lambda * Q)(t, t') = \delta^{\mathcal{C}}(t, t'), \quad (\text{A6b})$$

$$[i\partial_t^{\mathcal{C}} + \mu - U(t)]R(t, t') - (\Lambda * R)(t, t') = \delta^{\mathcal{C}}(t, t'), \quad (\text{A6c})$$

and boundary conditions (A4). For a quench the interaction is piecewise constant in time, $U(t) = \Theta(t)U_+ + \Theta(-t)U_-$. The effective medium propagator $\Lambda(t, t')$ must be determined self-consistently. For a semielliptic density of states of the mobile particles, which we adopt in the following, the self-consistency cycle can be condensed into closed form,²³

$$\Lambda(t, t') = V^2 G(t, t'), \quad (\text{A7})$$

where $2V$ is the half bandwidth of the density of states. Eqn. (A6) and (A7) form a complete set of equations for the local Green function. The local self-energy Σ of the mobile particles is then obtained from the Dyson equation of the local problem, $[(i\partial_t^{\mathcal{C}} + \mu)G(t, t') - [(\Lambda + \Sigma) * G](t, t') = \delta^{\mathcal{C}}(t, t')$. Together with Eq. (A6), this is easily transformed into

$$w_1 U(t) R(t, t') = (\Sigma * G)(t, t'). \quad (\text{A8})$$

Finally the local self-energy $\Sigma(t, t')$ is inserted into the lattice Dyson equation (A5),

$$(i\partial_t^{\mathcal{C}} + \mu - \epsilon_{\mathbf{k}})G_{\mathbf{k}}(t, t') - [\Sigma * G_{\mathbf{k}}](t, t') = \delta^{\mathcal{C}}(t, t'), \quad (\text{A9})$$

which yields the \mathbf{k} -dependent Green functions. Note that $G_{\mathbf{k}}(t, t')$ depends on momentum only via the single particle energy $\epsilon_{\mathbf{k}}$, because we assumed a homogeneous state.

3. Langreth rules

To solve the contour equations (A6b), (A6c), (A8), and (A9) we first rewrite them in terms of their retarded and lesser components, using the identities (A2). In effect, this means that contour derivatives $C(t, t') = \partial_t^{\mathcal{C}} A(t, t')$ are replaced by real-time derivatives,³⁸

$$C^r(t, t') = \partial_t A^r(t, t') \quad (\text{A10a})$$

$$C^<(t, t') = \partial_t A^<(t, t'), \quad (\text{A10b})$$

and convolutions $C(t, t') = [A * B](t, t')$ of two contour Green functions A and B are expressed in terms of their retarded, advanced, and lesser components according to the Langreth rules³⁸

$$C^r(t, t') = \int_{t'}^t d\bar{t} A^r(t, \bar{t}) B^r(\bar{t}, t'); \quad (\text{A11a})$$

$$C^<(t, t') = \int_{-\infty}^{t'} d\bar{t} A^<(t, \bar{t}) B^a(\bar{t}, t') + \int_{-\infty}^t d\bar{t} A^r(t, \bar{t}) B^<(\bar{t}, t'). \quad (\text{A11b})$$

The integral boundaries account for the fact that retarded (advanced) Green functions $A^{r(a)}(t, t')$ vanish when $t < t'$ ($t > t'$). Furthermore, we shifted $t_{\min} \rightarrow -\infty$ in the second equation, such that the convolution extends over the whole axis but contributions from the vertical part at $t_{\min} - i\tau$ can be dropped. This step is discussed in further detail below.

The contour delta function on the right-hand-side of (A6b), (A6c), and (A9) vanishes when the lesser component is taken, and it is replaced by the usual delta function $\delta(t - t')$ for the retarded components. However, because any retarded function $A^r(t, t')$ vanishes for $t < t'$, retarded equations of motion are only considered for $t > t'$, and the initial value at $t = t'$ is determined by the weight of the delta function and the derivative operator. In particular, we obtain

$$G_{\mathbf{k}}^r(t, t) = R^r(t, t) = Q^r(t, t) = -i \quad (\text{A12})$$

from Eqn. (A6b), (A6c), and (A9). These conditions follow also directly from the anticommutation relation of creation and annihilation operators.

4. Stationary states

For the interaction quench we treat the equations of motion separately in the four regions where both t and t' do not change sign; we introduce additional subscripts $+$ and $-$ which indicate whether the time arguments are

greater or less than zero, respectively. Inserting (A10a) and (A11a) into Eq. (A6) yields a closed set of equations for $R^r(t, t')$ and $Q^r(t, t')$,

$$\Lambda^r(t, t') = V^2[w_1 R^r(t, t') + w_0 Q^r(t, t')] \quad (\text{A13a})$$

$$[i\partial_t + \mu]Q^r(t, t') = \int_{t'}^t d\bar{t} \Lambda^r(t, \bar{t})Q^r(\bar{t}, t') \quad (\text{A13b})$$

$$[i\partial_t + \mu - U(t)]R^r(t, t') = \int_{t'}^t d\bar{t} \Lambda^r(t, \bar{t})R^r(\bar{t}, t'), \quad (\text{A13c})$$

which must be solved for $t > t'$, using the initial condition (A12). The self-consistency equation (A7) was used in Eq. (A13a). Note that in Eq. (A13), Green functions with both time arguments greater or less than zero, i.e., the $(++)$ and $(--)$ components, do not mix with other components. Because $U(t)$ is constant for $t > 0$ and $t < 0$, respectively, the solutions of (A13) are thus translationally invariant in time when both t and t' have the same sign, and we make the ansatz

$$A_{\pm\pm}^r(t, t') = a_{\pm}^r(t - t') \quad (\text{A14a})$$

$$\tilde{a}_{\pm}^r(z) = \int_0^\infty ds e^{izs} a_{\pm}^r(s) \quad (\text{A14b})$$

for all contour functions $A = G, R, Q, \Lambda, G_{\mathbf{k}}$, and Σ (with $a = g, r, q, \lambda, g_{\mathbf{k}}$, and σ , respectively). Using this ansatz in Eq. (A13) we obtain a set of cubic equations,

$$\tilde{g}_{\pm}^r(z) = w_0 \tilde{q}_{\pm}^r(z) + w_1 \tilde{q}_{\pm}^r(z), \quad (\text{A15a})$$

$$\tilde{q}_{\pm}^r(z) = [z + \mu - V^2 \tilde{g}_{\pm}^r(z)]^{-1} \quad (\text{A15b})$$

$$\tilde{r}_{\pm}^r(z) = [z + \mu - V^2 \tilde{g}_{\pm}^r(z) - U_{\pm}]^{-1}. \quad (\text{A15c})$$

that can be solved analytically. These cubic equations are well-known from the DMFT solution of the Falicov-Kimball model in equilibrium.³⁵ This is of course expected when both t and $t' < 0$, because before the quench the system indeed is in an equilibrium state. In a similar way, the retarded $(++)$ and $(--)$ components of Σ and $G_{\mathbf{k}}$ are obtained from Eq. (A8) and (A9),

$$\tilde{\sigma}_{\pm}^r(z) = w_1 U_{\pm} \tilde{r}_{\pm}^r(z) / \tilde{g}_{\pm}^r(z) \quad (\text{A16})$$

$$\tilde{g}_{\mathbf{k}\pm}^r(z) = [z + \mu - \epsilon_{\mathbf{k}} - \tilde{\sigma}_{\pm}^r(z)]^{-1}. \quad (\text{A17})$$

Furthermore, advanced Green functions are directly related to the retarded ones by symmetry (A3), so that we have

$$A_{\pm\pm}^a(t, t') = a_{\pm}^a(t - t') \quad (\text{A18a})$$

$$\tilde{a}_{\pm}^a(z) = \int_{-\infty}^0 ds e^{izs} a_{\pm}^a(s) = \tilde{a}_{\pm}^r(z^*)^*. \quad (\text{A18b})$$

The lesser Green functions are translationally invariant in time only for both t and $t' < 0$ [$(--)$ component], when the system is still in equilibrium. One then has³⁸

$$A_{--}^<(t, t') = \int \frac{d\omega}{2\pi} e^{i\omega(t'-t)} \tilde{a}_{-}^<(\omega), \quad (\text{A19a})$$

$$\tilde{a}_{-}^<(\omega) = f(\omega)[\tilde{a}_{-}^a(\omega) - \tilde{a}_{-}^r(\omega)], \quad (\text{A19b})$$

where $f(\omega) = 1/(e^{\omega/T} + 1)$ is the Fermi function, and $\tilde{a}_{-}^a(\omega) - \tilde{a}_{-}^r(\omega) = -2i \text{Im} a_{-}^r(\omega)$ is proportional to the spectrum of the equilibrium Green function. Mathematically this follows from the solutions of the equations of motion on the full contour, including the vertical part, and taking into account the antiperiodic boundary conditions. For the quench we use (A19) as *initial condition* for the lesser components; only then can we then let $t_{\min} \rightarrow -\infty$, and disregard the vertical part in the Langreth rule (A11b).

On the other hand, we show below that in the limit where both t and t' tend to ∞ (but their difference is finite), the lesser $(++)$ components take a form very similar to (A19),

$$\lim_{t \rightarrow \infty} A_{++}^<(t + s, t) = \int \frac{d\omega}{2\pi} e^{-i\omega s} \tilde{a}_{+}^<(\omega), \quad (\text{A20a})$$

$$\tilde{a}_{+}^<(\omega) = F(\omega)[\tilde{a}_{+}^a(\omega) - \tilde{a}_{+}^r(\omega)]. \quad (\text{A20b})$$

The function $F(\omega)$ is common for all $a = g, r, q, \sigma$, and $g_{\mathbf{k}}$. One can in fact directly see from the equations of motion (A6b), (A6c), (A8), and (A9) for the lesser component that *if* the stationary limit (A20a) exists, *then* Green functions $\tilde{a}_{+}^<(\omega)$ must have this common factor $F(\omega)$. To find this factor, however, the equations of motion must be solved, because it contains the entire information about the initial state.

5. Double Fourier transforms

We now consider the cases with one or two positive time arguments, i.e., after the quench. We introduce double Fourier transforms

$$\tilde{A}_{+-}^r(z, \eta) = \int_0^\infty dt e^{izt} \int_{-\infty}^0 dt' e^{i\eta t'} A_{+-}^r(t, t') \quad (\text{A21a})$$

$$\tilde{A}_{-+}^a(\eta, z) = \int_0^\infty dt e^{izt} \int_{-\infty}^0 dt' e^{i\eta t'} A_{-+}^a(t', t), \quad (\text{A21b})$$

for retarded and advanced components,

$$\int \frac{d\omega}{2\pi} e^{-i\omega t'} \tilde{A}_{+-}^<(z, \omega) = \int_0^\infty dt e^{izt} A_{+-}^<(t, t') \quad (\text{A22a})$$

$$\int \frac{d\omega}{2\pi} e^{-i\omega t'} \tilde{A}_{-+}^<(\omega, z) = \int_0^\infty dt e^{izt} A_{-+}^<(t', t) \quad (\text{A22b})$$

for the lesser components with mixed time arguments (which holds for $t' < 0$), and

$$\tilde{A}_{++}^<(z, \eta) = \int_0^\infty dt e^{izt} \int_0^\infty dt' e^{i\eta t'} A_{++}^<(t, t') \quad (\text{A23})$$

for the lesser Green function with both time arguments after the quench. In this subsection we derive explicit expressions for $\tilde{A}_{+-}^r(z, \omega)$, $\tilde{A}_{-+}^<(z, \omega)$, and $\tilde{A}_{++}^<(z, \omega)$; the remaining are then obtained by symmetry (A3),

$$\tilde{A}_{-+}^a(\eta, z) = \tilde{A}_{+-}^r(-\eta^*, -z^*)^* \quad (\text{A24a})$$

$$\tilde{A}_{-+}^<(\omega, z) = -\tilde{A}_{+-}^<(-z^*, -\omega)^*. \quad (\text{A24b})$$

Using Langreth rules (A11) once again yields for convolutions $C = A * B$,

$$\tilde{C}_{+-}^r(z, -\omega) = \tilde{A}_{+-}^r(z, -\omega)\tilde{b}_-^r(\omega) + \tilde{a}_+^r(z)\tilde{B}_{+-}^r(z, -\omega) \quad (\text{A25a})$$

$$\tilde{C}_{+-}^<(z, -\omega) = \tilde{A}_{+-}^<(z, -\omega)\tilde{b}_-^a(\omega) + \tilde{a}_+^r(z)\tilde{B}_{+-}^<(z, -\omega) + \tilde{A}_{+-}^r(z, -\omega)\tilde{b}_-^<(\omega) \quad (\text{A25b})$$

$$\tilde{C}_{++}^<(z, \eta) = \tilde{A}_{++}^<(z, \eta)\tilde{b}_+^a(-\eta) + \tilde{a}_+^r(z)\tilde{B}_{++}^<(z, \eta) + \int \frac{d\omega}{2\pi} [\tilde{A}_{+-}^<(z, -\omega)\tilde{B}_{+-}^a(\omega, \eta) + \tilde{A}_{+-}^r(z, -\omega)\tilde{B}_{+-}^<(\omega, \eta)]. \quad (\text{A25c})$$

Furthermore, the derivative $C = \partial_t^C A(t, t')$ translates into

$$\tilde{C}_{+-}^r(z, \eta) = z\tilde{A}^r(z, \eta) - i\tilde{a}_-^r(-\eta) \quad (\text{A26a})$$

$$\tilde{C}_{+-}^<(z, \omega) = z\tilde{A}_{+-}^<(z, -\omega) - i\tilde{a}_-^<(\omega) \quad (\text{A26b})$$

$$\tilde{C}_{++}^<(z, \eta) = z\tilde{A}_{++}^<(z, \eta) - i \int \frac{d\omega}{2\pi} \tilde{A}_{+-}^<(\omega, \eta), \quad (\text{A26c})$$

where one must use the continuity of the components at the boundary $t = 0$ and $t' = 0$, e.g., $A_{+-}^r(0, t') = A_{+-}^r(0, t')$.

Using (A25) and (A26) one can rewrite Eq. (A6) for the various components and solve them using the self-consistency equation (A7). For instance, we obtain the $(+-)$ component of the retarded Green functions as

$$\tilde{R}_{+-}^r(z, \eta) = [\tilde{\Lambda}_{+-}^r(z, \eta) + i]r_+^r(z)r_-^r(-\eta), \quad (\text{A27})$$

$$\tilde{Q}_{+-}^r(z, \eta) = [\tilde{\Lambda}_{+-}^r(z, \eta) + i]q_+^r(z)q_-^r(-\eta), \quad (\text{A28})$$

where Eq. (A15) was used once. Together with the self-consistency (A7), this is a simple linear equation for $\Lambda_{+-}^r(z, \eta)$. In a similar way all components are determined successively: Starting from the retarded $(+-)$ and advanced $(-+)$ components, the results enter the lesser $(+-)$ and lesser $(-+)$ components [cf. Eqn. (A25b) and (A26b)], which in turn enter the equations for the lesser $(++)$ component [cf. Eqn. (A25c) and (A26c)]. The procedure is repeated for Eq. (A6), Eq. (A8), and finally for the lattice Dyson equation (A9), which yields the momentum-dependent Green function $G_{\mathbf{k}}(t, t')$.

For completeness we state the final result for G , R , and $G_{\mathbf{k}}$. For this we introduce the abbreviations

$$M_{\alpha\beta}^{xy} = [1 - V^2(w_1\tilde{r}_\alpha^x\tilde{r}_\beta^y + w_0\tilde{q}_\alpha^x\tilde{q}_\beta^y)]^{-1}, \quad (\text{A29a})$$

$$\kappa_\alpha^x = \tilde{r}_\alpha^x\tilde{q}_\alpha^x/\tilde{g}_\alpha^x. \quad (\text{A29b})$$

$$K_{\alpha\beta}^{xy} = 1 + w_1w_0U_+U_-\kappa_\alpha^x\kappa_\beta^yM_{\alpha\beta}^{xy}, \quad (\text{A29c})$$

with superscripts $x, y \in \{r, a\}$, and subscripts $\alpha, \beta \in \{+, -\}$, and we use the convention that the variables of a function a_α^x is (i) z when $x = r$ and $\alpha = +$, (ii) $-\eta$ when $x = a$ and $\alpha = +$, and (iii) ω when $\alpha = -$. In terms of

these expressions the final result is

$$\tilde{G}_{+-}^r(z, -\omega) = iV^{-2}(M_{+-}^{rr} - 1), \quad (\text{A30a})$$

$$\tilde{R}_{+-}^r(z, -\omega) = i\tilde{r}_+^r\tilde{r}_-^rM_{+-}^{rr}, \quad (\text{A30b})$$

$$\tilde{G}_{\mathbf{k}+-}^r(z, -\omega) = i\tilde{g}_{\mathbf{k}+}^r\tilde{g}_{\mathbf{k}-}^rK_{+-}^{rr}, \quad (\text{A30c})$$

and

$$\tilde{G}_{+-}^<(z, -\omega) = if(\omega)(M_{+-}^{ra} - M_{+-}^{rr})/V^2, \quad (\text{A31a})$$

$$\tilde{R}_{+-}^<(z, -\omega) = if(\omega)\tilde{r}_+^r(\tilde{r}_+^aM_{+-}^{ra} - \tilde{r}_-^rM_{+-}^{rr}), \quad (\text{A31b})$$

$$\tilde{G}_{\mathbf{k}+-}^<(z, -\omega) = if(\omega)\tilde{g}_{\mathbf{k}+}^r(\tilde{g}_{\mathbf{k}-}^aK_{+-}^{ra} - \tilde{g}_{\mathbf{k}-}^rK_{+-}^{rr}). \quad (\text{A31c})$$

The lesser $(++)$ component can be written in the form

$$A_{++}^<(z, \eta) = \tilde{F}(z, \eta)\frac{\tilde{a}_+^a - \tilde{a}_+^r}{\eta + z} + F_A(z, \eta) \quad (\text{A32a})$$

for $A = G, R$, and $G_{\mathbf{k}}$, where

$$\tilde{F}(z, \eta) = \int \frac{d\omega}{2\pi} f(\omega)\frac{M_{+-}^{rr} + M_{+-}^{aa} - M_{+-}^{ra} - M_{+-}^{ar}}{z + \eta + V^2(\tilde{g}_+^a - \tilde{g}_+^r)}, \quad (\text{A32b})$$

and

$$F_G(z, \eta) = \tilde{F}(z, \eta)/V^2, \quad (\text{A32c})$$

$$F_R(z, \eta) = \tilde{r}_+^r\tilde{r}_+^a \int \frac{d\omega}{2\pi} f(\omega) \times (\tilde{r}_-^aM_{+-}^{aa}M_{+-}^{ra} - \tilde{r}_-^rM_{+-}^{rr}M_{+-}^{ar}), \quad (\text{A32d})$$

$$F_{G_{\mathbf{k}}}(z, \eta) = \tilde{g}_{\mathbf{k}+}^r\tilde{g}_{\mathbf{k}+}^a \left\{ -\tilde{F}(z, \eta) + \int \frac{d\omega}{2\pi} f(\omega) \times \left[w_0w_1U_+^2\tilde{\kappa}_+^r\tilde{\kappa}_+^a(\tilde{\kappa}_-^aM_{+-}^{aa}M_{+-}^{ra} - \tilde{\kappa}_-^rM_{+-}^{rr}M_{+-}^{ar}) + \tilde{g}_{\mathbf{k}-}^aK_{+-}^{aa}K_{+-}^{ra} - \tilde{g}_{\mathbf{k}-}^rK_{+-}^{rr}K_{+-}^{ar} \right] \right\}. \quad (\text{A32e})$$

6. Back transformation

To obtain the physical real-time Green functions, we have to invert the double Fourier transformations (A21),

(A22), and (A23), using the final expressions (A29) through (A32). Here we give an explicit formula for the partially Fourier-transformed lesser component

$$\tilde{A}^<(\omega, t) = \int ds e^{i\omega s} A^<(t + s, t), \quad (\text{A33})$$

($A = G, R,$ and $G_{\mathbf{k}}$). The singularity at $\eta + z = 0$ in Eq. (A32a) determines (A33) in the limit $t \rightarrow \infty$,

$$\begin{aligned} \tilde{a}_{\pm}^<(\omega) &\equiv \lim_{t \rightarrow \infty} \tilde{A}^<(\omega, t) \\ &= \text{Im} \tilde{F}(\omega, -\omega) [\tilde{a}_{\pm}^{\text{a}}(\omega) - \tilde{a}_{\pm}^{\text{r}}(\omega)], \end{aligned} \quad (\text{A34})$$

which is of the form discussed above [cf. Eq. (A20)], with $F(\omega) = \text{Im} \tilde{F}(\omega, -\omega)$. The full result is given by

$$\begin{aligned} \tilde{A}^<(\omega, t) &= \sum_{\pm} \Theta(\pm t) \\ &\times \left[\tilde{a}_{\pm}^<(\omega) + e^{-i\omega t} \int \frac{d\eta}{2\pi} e^{-i\eta} \hat{A}_{\pm}(\omega, \eta) \right], \end{aligned} \quad (\text{A35a})$$

where

$$\hat{A}_{-}(\omega, \eta) = \tilde{A}_{+-}^<(\omega, \eta) + \frac{\tilde{a}_{-}^<(-\eta) - \tilde{a}_{-}^<(\omega)}{i(\eta + \omega)}, \quad (\text{A35b})$$

$$\begin{aligned} \hat{A}_{+}(\omega, \eta) &= 2i \text{Im} \frac{\tilde{F}(\omega, \eta) [\tilde{a}_{+}^{\text{a}}(-\eta) - \tilde{a}_{+}^{\text{r}}(\omega)]}{\omega + \eta} \\ &+ F_A(\omega, \eta) + \int \frac{d\omega'}{2\pi i} \frac{\tilde{A}_{-+}^<(\omega', \eta)}{\omega - i0 - \omega'}, \end{aligned} \quad (\text{A35c})$$

and the components for $A = G, R,$ and $G_{\mathbf{k}}$ were given in the previous subsection. Note that the first term on the right hand side of Eq. (A35c) is regular at $\eta = -\omega$, because both $\tilde{F}(\omega, \eta)$ and $\tilde{a}_{+}^{\text{a}}(-\eta) - \tilde{a}_{+}^{\text{r}}(\omega)$ are then purely imaginary.

-
- ¹ A. H. Zewail, *J. Phys. Chem. A* **104**, 5660 (2000).
² W. M. Axt and T. Kuhn, *Rep. Prog. Phys.* **67**, 433 (2004).
³ H. Petek and S. Ogawa, *Prog. in Surf. Sci.* **56**, 239 (1997).
⁴ T. Ogasawara, M. Ashida, N. Motoyama, H. Eisaki, S. Uchida, Y. Tokura, H. Ghosh, A. Shukla, S. Mazumdar, and M. Kuwata-Gonokami, *Phys. Rev. Lett.* **85**, 2204 (2000).
⁵ S. Iwai, M. Ono, A. Maeda, H. Matsuzaki, H. Kishida, H. Okamoto, and Y. Tokura, *Phys. Rev. Lett.* **91**, 057401 (2003).
⁶ M. Chollet, L. Guerin, N. Uchida, S. Fukaya, H. Shimoda, T. Ishikawa, K. Matsuda, T. Hasegawa, A. Ota, H. Yamochi, G. Saito, R. Tazaki, S. Adachi, and S. Koshihara, *Science* **307**, 86 (2005).
⁷ L. Perfetti, P. A. Loukakos, M. Lisowski, U. Bovensiepen, H. Berger, S. Biermann, P. S. Cornaglia, A. Georges and M. Wolf, *Phys. Rev. Lett.* **97**, 067402 (2006); L. Perfetti, P. A. Loukakos, M. Lisowski, U. Bovensiepen, M. Wolf, H. Berger, S. Biermann, and A. Georges, *New. J. Phys.* **10**, 053019 (2007).
⁸ H. Okamoto, H. Matsuzaki, T. Wakabayashi, T. Takahashi, and T. Hasegawa, *Phys. Rev. Lett.* **98**, 037401 (2007).
⁹ C. Kübler, H. Ehrke, R. Huber, A. Halabica, R. F. Haglung, J. Leitenstorfer, and A. Leitenstorfer, *Phys. Rev. Lett.* **99**, 116401 (2007).
¹⁰ M. Imada, A. Fujimori, and Y. Tokura, *Rev. Mod. Phys.* **70**, 1039 (1998).
¹¹ P. B. Allen, *Phys. Rev. Lett.* **59**, 1460 (1987).
¹² J. K. Freericks, H. R. Krishnamurthy, Y. Ge, A. Y. Lu, and Th. Pruschke, arXiv:0809.2347.
¹³ W. S. Fann, R. Storz, H. W. K. Tom and J. Bokor, *Phys. Rev. Lett.* **68**, 2834 (1992).
¹⁴ G. Steinmeyer, D. H. Sutter, L. Gallmann, N. Matuschek, and U. Keller, *Science* **286**, 1507 (1999).
¹⁵ M. Hentschel, R. Kienberger, Ch. Spielmann, G. A. Reider, N. Milosevic, T. Brabec, P. Corkum, U. Heinzmann, M. Drescher, F. Krausz, *Nature* **414**, 509 (2001).
¹⁶ A. L. Cavalieri, N. Müller, Th. Uphues, V. S. Yakovlev, A. Baltuska, B. Horvath, B. Schmidt, L. Blümel, R. Holzwarth, S. Hendel, M. Drescher, U. Kleineberg, P. M. Echenique, R. Kienberger, F. Krausz, and U. Heinzmann, *Nature* **449**, 1029 (2007).
¹⁷ W. Schattke and M. A. van Hove, *Solid-State Photoemission and Related Methods*, Wiley-VCH (Weinheim, 2003).
¹⁸ F. Reinert and S. Hüfner, *New J. Phys.* **7**, 97 (2005).
¹⁹ J. K. Freericks, H. R. Krishnamurthy, and Th. Pruschke, arXiv:0806.4781.
²⁰ M. Sakaue, T. Munakat, H. Kasai, and A. Okiji, *Phys. Rev. B* **66**, 094302 (2002).
²¹ A. Georges, G. Kotliar, W. Krauth, and M. J. Rozenberg, *Rev. Mod. Phys.* **68**, 13 (1996).
²² J. K. Freericks, V. M. Turkowski, and V. Zlatić, *Phys. Rev. Lett.* **97**, 266408 (2006); J. K. Freericks, *Phys. Rev. B* **77**, 075109 (2008).
²³ M. Eckstein and M. Kollar, *Phys. Rev. Lett.* **100**, 120404 (2008).
²⁴ N. Tsuji, T. Oka, and H. Aoki, arXiv:0808.0379.
²⁵ M. Eckstein and M. Kollar, arXiv:0808.1005.
²⁶ M.-T. Tran, *Phys. Rev. B* **78**, 125103 (2008).
²⁷ W. Metzner and D. Vollhardt, *Phys. Rev. Lett.* **62**, 324 (1989).
²⁸ L. M. Falicov and J. C. Kimball, *Phys. Rev. Lett.* **22**, 997 (1969).
²⁹ M. Greiner, O. Mandel, Th. W. Hänsch, and I. Bloch, *Nature* **419**, 51 (2002).
³⁰ A short pulse has necessarily finite extent in space, but its spread in wavenumber can nevertheless be neglected due to the steep dispersion of light: even when the frequency width of the pulse is on the order of a typical bandwidth ($\hbar\delta\omega = 1 \text{ eV}$), the spread in wavenumber, $\delta q = |\delta\omega/c| \approx 0.0005/\text{\AA}$, which is small compared to the typical extent of

the Brillouin zone.

- ³¹ L. Hedin and J. D. Lee, *J. of Elec. Spec. and Rel. Phen.* **124**, 289 (2002).
- ³² L. P. Kadanoff and G. Baym, *Quantum Statistical Mechanics* (W. A. Benjamin, New York, 1962).
- ³³ U. Brandt and C. Mielsch, *Z. Phys. B* **75**, 365 (1989).
- ³⁴ J. K. Freericks and V. Zlatić, *Rev. Mod. Phys.* **75**, 1333 (2003).
- ³⁵ P. G. J. van Dongen and D. Vollhardt, *Phys. Rev. Lett.* **65**, 1663 (1990).
- ³⁶ P. G. J. van Dongen, *Phys. Rev. B* **45**, 2267 (1992).
- ³⁷ L. V. Keldysh, *J. Exptl. Theoret. Phys.* **47**, 1515 (1964) [*Sov. Phys. JETP* **20**, 1018 (1965)].
- ³⁸ For an introduction see H. Haug and A.-P. Jauho, *Quantum Kinetics in Transport and Optics of Semiconductors* (Springer, Berlin, 1996).